doi:10.1016/j.jmb.2010.05.050 J. Mol. Biol. (2010) 400, 922–934

JMB

Available online at www.sciencedirect.com

ScienceDirect

ELSEVIER

Design and Structure of an Equilibrium Protein Folding Intermediate: A Hint into Dynamical Regions of Proteins

Sara Ayuso-Tejedor[1,2,3], Vladimir Espinosa Angarica[1,2,3], Marta Bueno[1,2,3], Luis A. Campos[1,2,3], Olga Abián[2,3,4], Pau Bernadó[5], Javier Sancho[1,2,3]* and M. Angeles Jiménez[6]*

[1]*Departamento de Bioquímica y Biología Molecular y Celular, Facultad de Ciencias, Universidad de Zaragoza, 50009 Zaragoza, Spain*

[2]*Biocomputation and Complex Systems Physics Institute (BIFI), Universidad de Zaragoza, 50009 Zaragoza, Spain*

[3]*Unidad Asociada BIFI-IQFR, CSIC, Spain*

[4]*H.C.U. Lozano Blesa, Instituto Aragonés de Ciencias de la Salud (I+CS-CIBEREHD), 50009 Zaragoza, Spain*

[5]*Institute for Research in Biomedicine, Parc Científic de Barcelona, Baldiri Reixac, 10 08028 Barcelona, Spain*

[6]*Instituto de Química-Física Rocasolano, CSIC, Serrano 119, 28006 Madrid, Spain*

Received 17 March 2010; received in revised form 13 May 2010; accepted 21 May 2010
Available online 27 May 2010

Edited by K. Kuwajima

Partly unfolded protein conformations close to the native state may play important roles in protein function and in protein misfolding. Structural analyses of such conformations which are essential for their fully physicochemical understanding are complicated by their characteristic low populations at equilibrium. We stabilize here with a single mutation the equilibrium intermediate of apoflavodoxin thermal unfolding and determine its solution structure by NMR. It consists of a large native region identical with that observed in the X-ray structure of the wild-type protein plus an unfolded region. Small-angle X-ray scattering analysis indicates that the calculated ensemble of structures is consistent with the actual degree of expansion of the intermediate. The unfolded region encompasses discontinuous sequence segments that cluster in the 3D structure of the native protein forming the FMN cofactor binding loops and the binding site of a variety of partner proteins. Analysis of the apoflavodoxin inner interfaces reveals that those becoming destabilized in the intermediate are more polar than other inner interfaces of the protein. Natively folded proteins contain hydrophobic cores formed by the packing of hydrophobic surfaces, while natively unfolded proteins are rich in polar residues. The structure of the apoflavodoxin thermal intermediate suggests that the regions of natively folded proteins that are easily responsive to thermal activation may contain cores of intermediate hydrophobicity.

Keywords: folding intermediate; protein design; protein structure; NMR; SAXS

Introduction

Important events in the function of proteins, such as ligand binding or catalysis, may require the transient population of conformations out of equilibrium, which are likely to be distorted or locally unfolded native states.[1–3] For an efficient sampling of an unfolded or partly unfolded conformation, its free energy should be close to that of the native state.[4] This energetic proximity may allow partly

*Corresponding authors. E-mail addresses: jsancho@unizar.es; majimenez@iqfr.csic.es.

Abbreviations used: SAXS, small-angle X-ray scattering; DSC, differential scanning calorimetry; HSQC, heteronuclear single quantum coherence; NOE, nuclear Overhauser enhancement; NOESY, nuclear Overhauser enhancement spectroscopy; BioMagResBank, Biological Magnetic Resonance Data Bank; PDB, Protein Data Bank.

unfolded forms to become more stable than the native state under a variety of stress conditions such as high temperature or point mutations. It is even possible that aggregative processes of proteins start from partly unfolded conformations and, in this respect, protein aggregation might be considered as a side effect of protein function. A detailed structural and energetic characterization of partly unfolded conformations is crucial for understanding protein dynamics and the early stages of protein aggregation. At present, the structure of partly unfolded conformations of proteins can be investigated in some detail by NMR[5–12] and protein engineering.[12–15]

Apoflavodoxins are one-domain proteins that have been used as models in protein stability, folding, and binding studies.[16] In thermal unfolding, they typically populate an intermediate conformation in equilibrium with the native and the fully unfolded states. The equilibrium intermediates of the apoflavodoxins from *Anabaena* PCC 7119[13,14,17] and *Helicobacter pylori*[18,19] are only 1.5–2.0 kcal/mol less stable than the corresponding native states. The equivalent intermediate of *Azotobacter vinelandii* apoflavodoxin[20] en detected by NMR as a major partly unfolded form. According to equilibrium ϕ-analysis,[14] the *Anabaena* intermediate contains a large native-like region comprising most helices and β-strands of the native state and a smaller unfolded region encompassing one β-strand and several loops that are close in the tridimensional structure of the native protein. During thermal unfolding, the intermediate never populates to more than 65% and it is thus difficult to characterize by NMR. Nevertheless, it has been shown that it does not resemble other equilibrium or transient conformations adopted by the protein under a variety of conditions, such as the low-pH molten globule[21] or the transition state of folding.[22,23]

Based on the qualitative structural model of the apoflavodoxin thermal intermediate,[14] we have designed a point mutant at the interface between the native-like and the disordered regions. As intended by design, at 25 °C, the mutant exhibits the spectroscopic properties of the thermal intermediate of wild-type apoflavodoxin and follows a simple two-state thermal unfolding mechanism, and importantly, the accompanying population of denatured state is negligible, which facilitates NMR studies. The solution structure of this intermediate determined by NMR and consistent with small-angle X-ray scattering (SAXS) data reveals at great detail the boundary between a large native region and a smaller disordered one. In the context of the native protein, the buried interface between the two regions is singularized by its comparatively high polarity.

Results

Rational design of a stable model of the wild-type apoflavodoxin intermediate

Native *Anabaena* apoflavodoxin contains a buried hydrophobic cluster composed of four aromatic residues. One of them, F98, belongs to a small cofactor binding loop, while the others (Y125, F127, and F138) are located in a long, neighboring loop, characteristic of the so-called long-chain flavodoxins, which appears to be implicated in function.[24,25] Our previously reported ϕ-analysis data[14] predict that the native aromatic cluster is not formed in the equilibrium intermediate because the two loops involved are unfolded.

To obtain an apoflavodoxin variant where the intermediate were the only conformation significantly populated at 25 °C, we have destabilized the native state by replacing one of the buried residues of the cluster, F98, by asparagine. Besides weakening the aromatic cluster, this mutation should additionally destabilize the native conformation because it brings a polar residue into the protein core. The mutation, however, should be fairly neutral for the intermediate because the aromatic cluster is already broken and because position 98 is likely solvent exposed in the intermediate. Since the free-energy difference between native and intermediate wild-type conformations is small, about 1.5 kcal/mol,[14] the specific destabilization of the native state achieved in the mutant is expected to leave the intermediate as the most stable and major species at 25 °C.

Spectroscopic and thermodynamic characterization of F98N apoflavodoxin

The conformation of the F98N mutant at 25 °C has been analyzed by near-UV and far-UV circular dichroism (CD) (Fig. 1) and compared with that of the wild-type apoflavodoxin intermediate. The thermal dependence of far- and near-UV CD spectra of the wild-type protein was examined within the 4–75 °C temperature range (Fig. 1). The pure spectra of the wild-type intermediate, which were derived from global fitting of those spectra to a three-state model, are similar to those recorded for F98N apoflavodoxin at 25 °C (Fig. 1). According to the spectra, most of the secondary structure is preserved in the intermediate and in the F98N mutant, while the tertiary interactions giving rise to the near-UV CD are only partially retained. The near-UV CD spectrum of F98N is, however, closer to that of the wild-type native protein than that of the thermal intermediate since, in the latter, the peaks characteristic of the native state are weaker than those in F98N. This suggests that F98N still has some side-chain packing interactions involving aromatic residues and that it may be structurally more organized than the thermal unfolding intermediate. Another potential contribution to the differences observed in the near-UV CD spectra of F98N and of the thermal intermediate of the wild-type protein is the fact that the spectrum of F98N was recorded at 25 °C while that of the intermediate has been inferred from a variety of spectra obtained at higher temperatures (see above).

The thermal unfolding of wild-type apoflavodoxin is three-state.[13,17] If F98N were structurally

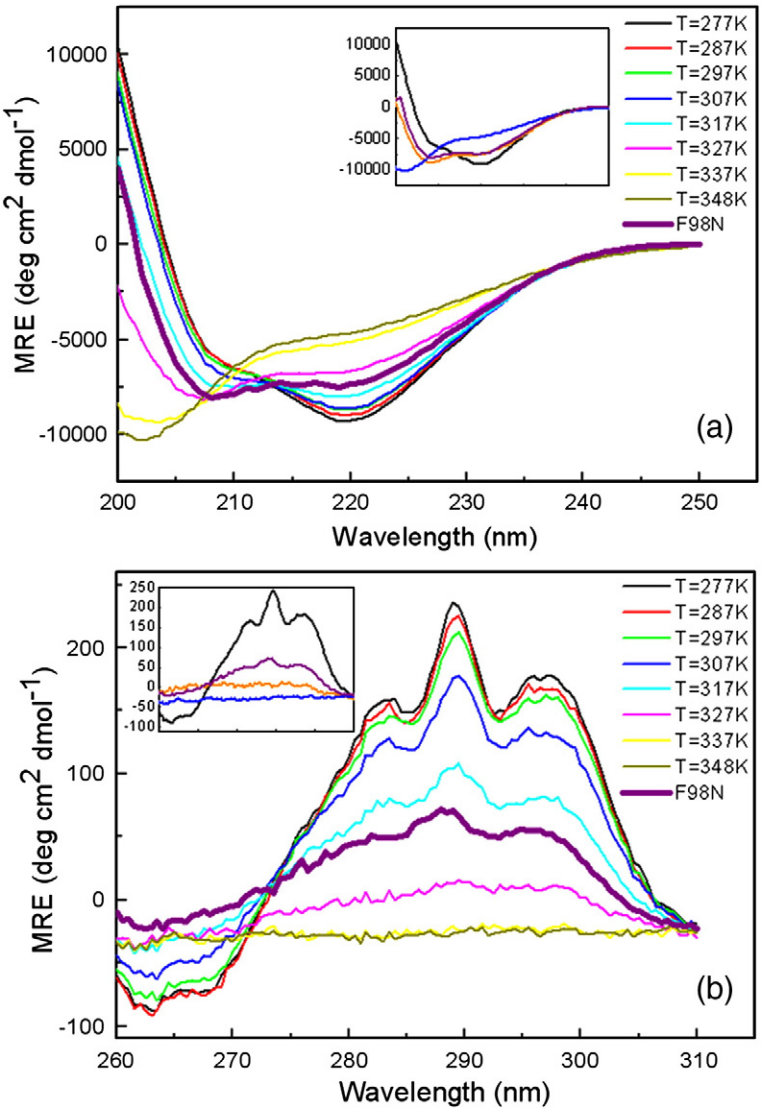

Fig. 1. Far-UV (top) and near-UV (bottom) CD spectra of wild-type apoflavodoxin at several temperatures (from 277 to 348 K) compared with the corresponding spectra of the F98N mutant at 298 K. The insets allow to compare the spectra of the F98N mutant (purple) with those calculated for the native (black), intermediate (orange), and fully denatured (blue) forms of wild-type apoflavodoxin.

similar to the wild-type intermediate, the F98N thermal unfolding should be two-state. To test this possibility, the thermal unfolding equilibrium of the mutant was followed by near- and far-UV CD, near-UV absorbance, and fluorescence emission, and the four curves were globally fitted (see Materials and Methods). While the equivalent global fit for the wild-type protein requires a three-state model,[13,14] the F98N curves can be satisfactorily fitted to a two-state model (Fig. 2a). Differential scanning calorimetry (DSC) was used to confirm the simple two-state model of F98N thermal unfolding. The F98N

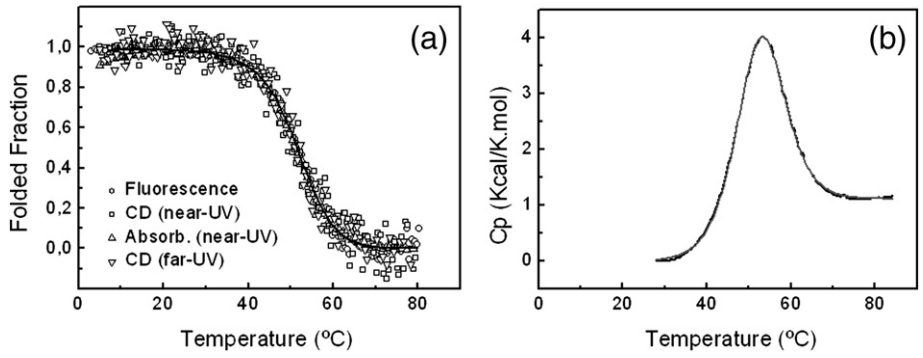

Fig. 2. Thermal unfolding of F98N apoflavodoxin followed using (a) several spectroscopic properties (fluorescence, near-UV CD, near-UV absorbance, and far-UV CD) and (b) DSC. The continuous line in (a) is a global fit of the four spectroscopic thermal unfolding curves to a two-state model. The continuous line in (b) is also a fit to a two-state model.

Table 1. Thermal unfolding equilibrium of wild-type and F98N apoflavodoxins

Protein	Technique	T_{m1} (K)	ΔH_1 (kcal/mol)	ΔC_p (kcal/mol)	T_{m2} (K)	ΔH_2 (kcal/mol)	ΔC_p (kcal/mol)
WT	Spectroscopy	317.2±0.3	32.2±0.4		328.9±0.1	51.0±1.1	
	DSC	317.1±0.6	32.7±1.3	1.2±0.1	329.4±0.1	66.0±0.2	1.5±0.1
F98N	Spectroscopy	—	—		324.2±0.1	46.3±0.9	
	DSC	—	—		324.2±0.1	51.2±0.2	1.4±0.2

Thermal unfolding of wild-type and F98N apoflavodoxin analyzed by spectroscopic and calorimetric techniques. The spectroscopic ΔH and T_m values are derived from global fits of four thermal unfolding curves recorded using fluorescence emission, near-UV CD, near-UV absorbance, and far-UV CD. Proteins were dissolved in 50 mM Mops, pH 7.0.

thermogram can be fitted to the two-state model (Fig. 2b), with a ratio of van't Hoff to calorimetric enthalpy close to 1. A three-state analysis of the thermogram does not significantly improve the fit.

The thermodynamic parameters obtained from the calorimetric and spectroscopic analyses of F98N thermal unfolding are presented in Table 1, where they are compared with those previously reported for the three-state analysis of the wild-type protein. The mid-temperature of denaturation of F98N lies between the two transition temperatures described for the wild-type protein, while the enthalpy change of denaturation of the mutant is quite close to that of the I-to-U transition of the wild-type protein.

NMR structural characterization of F98N

A comparison of the 2D NMR spectra of F98N apoflavodoxin with those of the wild-type protein evidences that some signals belonging to equivalent residues are located at close positions [see L44, V76, V160, and L163 signals in the 2D ^{1}H–^{13}C-heteronuclear single quantum coherence (HSQC) spectral region shown in Fig. 3a], whereas others appear to be absent in the mutant (see L141 and A142 cross-peaks in Fig. 3a), which reflects that their chemical shifts differ greatly from those in the wild-type protein. On the whole, the NMR spectra of F98N display less chemical shift dispersion and slightly broader signals and, hence, higher signal overlap than those of the wild-type protein, which makes resonance assignment a complex task. In spite of this, it was possible to unambiguously assign about 64% of the residues assigned in the wild-type protein. Except for a few cross-peaks for which assignment was ambiguous, unassigned signals in the 2D ^{1}H–^{15}N-HSQC (Fig. 3b) are found in a narrow spectral range, approximately 8.7–8.0 ppm and 123–118 ppm, respectively, at the ^{1}H and ^{15}N dimensions. Tentative assignments for some unassigned residues showed chemical shifts closer to the random-coil values than to those observed for the wild-type protein. These observations suggest that the two regions where the unassigned residues are located (87–108 and 118–152; Fig. 4a), and which are spatially close in the native apoflavodoxin structure, are mainly disordered. The assigned residues also belong to regions spatially close in the wild-type apoflavodoxin structure (Fig. 4a). The similarity of the chemical shifts of these residues in F98N and in wild-type apoflavodoxin indicates that these regions maintain the native structure. In brief, the qualitative picture of the F98N structure that arises from chemical shift analysis is that of a polypeptide containing a well-folded region with native-like structure together with some long disordered segments. This is supported by the fact that the nuclear Overhauser enhancements (NOEs) involving protons from the residues in the ordered regions are observed in wild-type native apoflavodoxin as well. Thus, the native parallel arrangement of the β-strands in F98N mutant is substantiated by the presence in the 2D NOE spectroscopy (NOESY) spectra of characteristic backbone cross-strand NOEs. Besides, many long-range NOEs involving side-chain protons identified in the 2D NOESY spectra of native apoflavodoxin are also found in the F98N mutant (Fig. 3c).

The 3D structure calculated using distance restraints derived from observed NOEs and ϕ and ψ dihedral constraints derived from chemical shifts agrees with our qualitative picture of the F98N structure. As expected, it contains both well-defined regions and very disordered ones (Fig. 4b). Thus, the average pairwise RMSD for all backbone atoms is 9.1±2.8 Å, but it goes down to 1.1±0.2 Å when only the ordered segments, residues 2–8, 18–53, 71–86, 109–117, and 153–169, are considered. Most of these 85 residues show also ordered side chains. The well-defined 85 residues represent around 50% of the protein. However, some residues at regions involved in cofactor binding could not be assigned in wild-type apoflavodoxin, probably due to being involved in slow exchange processes.[26] Therefore, those 85 natively folded residues found in the mutant constitute as much as two-thirds of the assigned residues in the native wild-type protein. The structure of the folded region in F98N is very similar to the wild-type structure, as seen in Fig. 4c and d (RMSD for the backbone atoms of the F98N folded region *versus* the crystalline wild-type structure is 3.0±0.1 Å). The main differences between the folded region of F98N and that of the wild type always occur at residues close to the disordered regions. In agreement with the CD data (Fig. 1a), most of the secondary-structure elements of the wild-type protein are preserved in the mutant.

Structural characterization of F98N by SAXS

SAXS is a well-suited technique to characterize the size and shape properties of biomolecules in

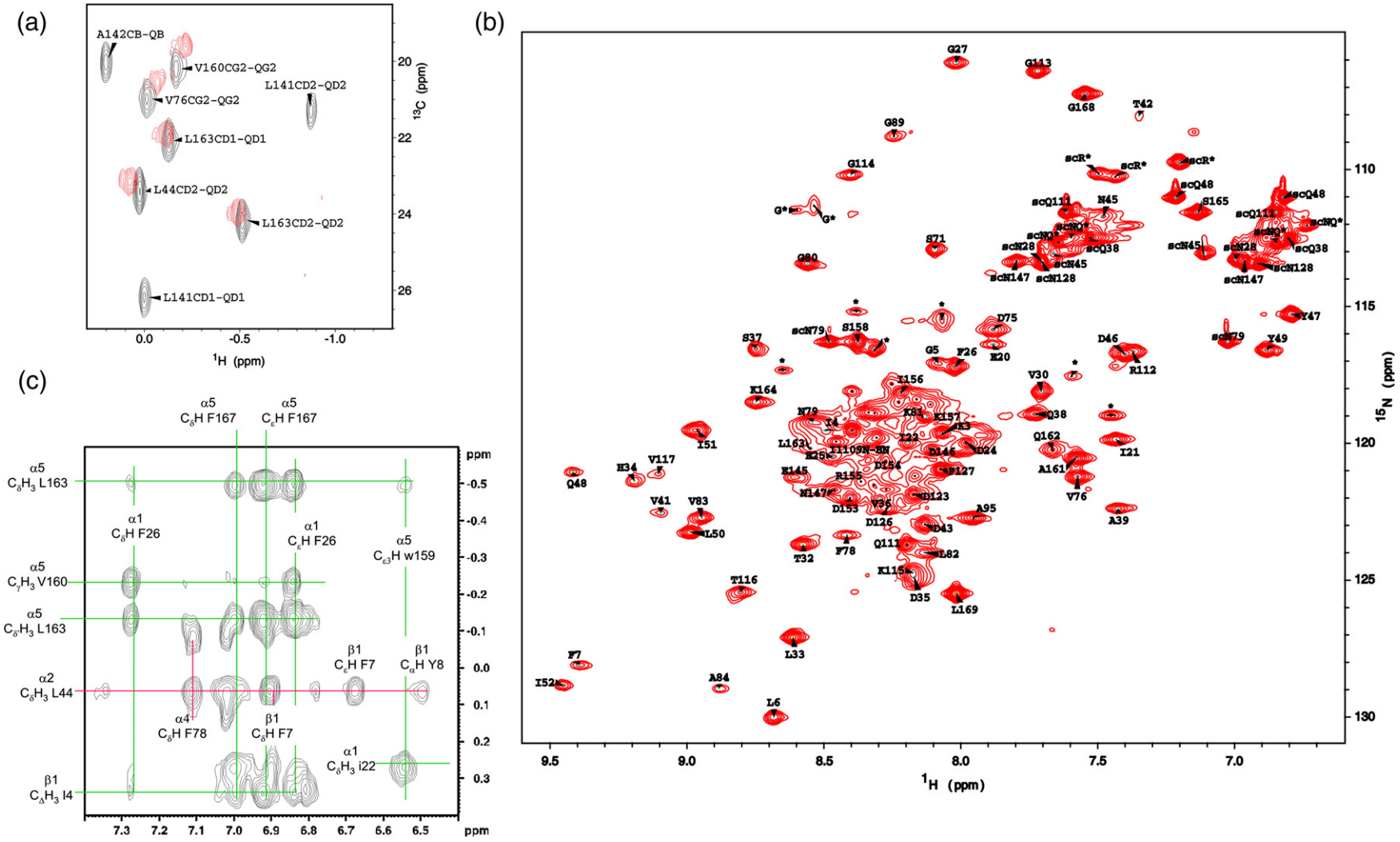

Fig. 3. Selected NMR spectral regions of F98N-apoflavodoxin at pH 7.0 and 25 °C. (a) ^{1}H,^{13}C-HSQC spectral region of F98N-apoflavodoxin in D_2O (in red) superimposed on that of the wild-type protein (in black) under similar experimental conditions. (b) ^{1}H,^{15}N-HSQC spectral region of F98N-apoflavodoxin in H_2O/D_2O 9:1 v/v. Labels indicate the assignment of the cross-peaks, asterisks designate unassigned cross-peaks, and "sc" means side chain of Gln, Asn, and Arg. (c) 2D-NOESY spectral region where many long-range NOE cross-peaks are observed. They are labeled.

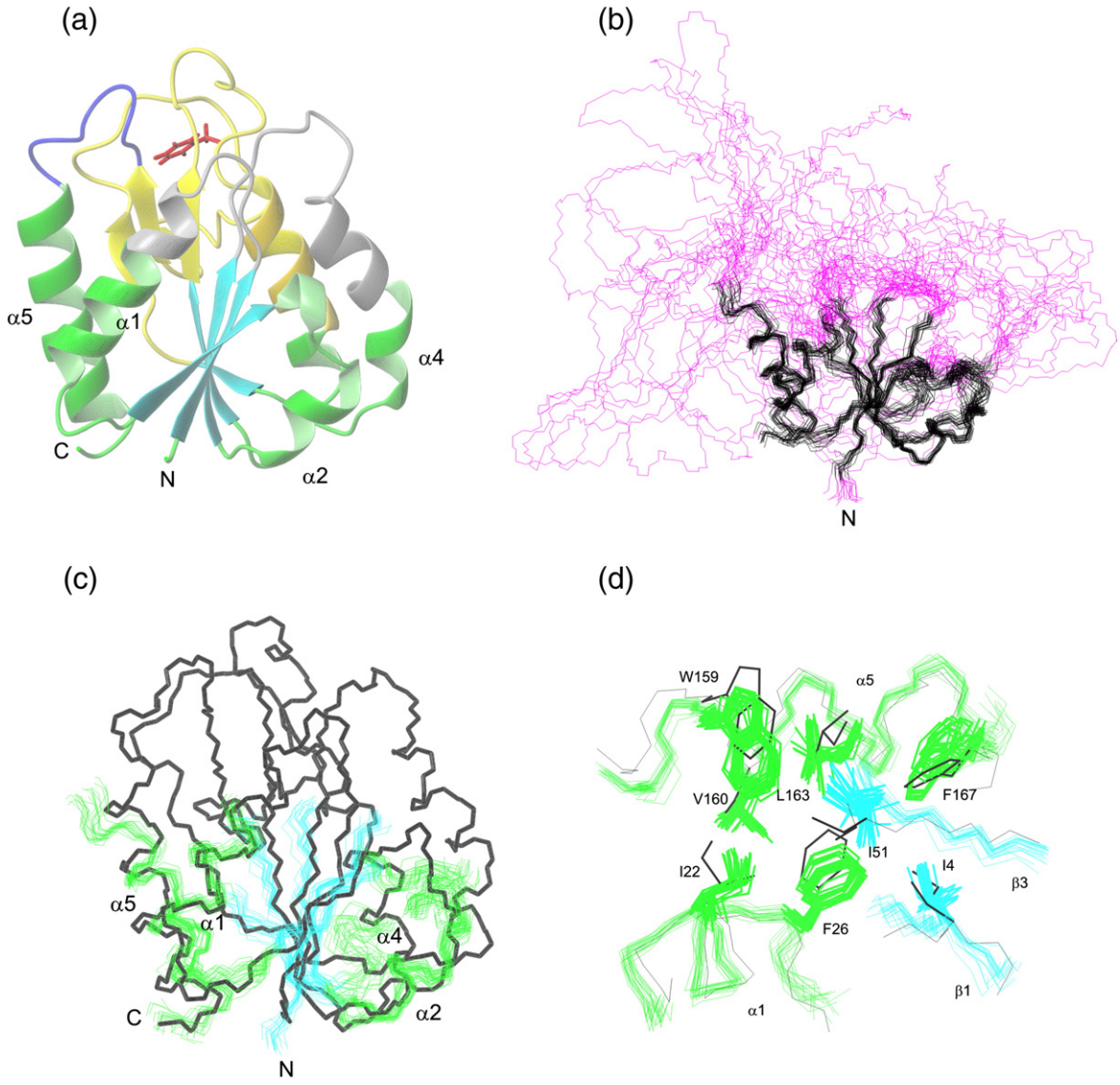

Fig. 4. 3D structures of the wild-type and F98N apoflavodoxins. (a) Ribbon representation of the wild-type apoflavodoxin structure (PDB code: 1FTG). Residues assigned for F98N-apoflavodoxin are displayed in green except for β-strands that are displayed in cyan; residues assigned for wild-type but not for F98N mutant are shown in yellow, and those not found in either wild-type or F98N mutant are in gray. The loop corresponding to residues 144–151, whose chemical shifts differ significantly between F98N mutant and wild-type protein, is in blue. Side-chain atoms for residue F98 are shown in red. (b) Backbone atoms of the structure calculated for F98N-apoflavodoxin superposed over residues 2–8, 18–53, 71–86, 109–117, and 153–169. Disordered regions are shown in magenta. (c) Well-folded regions in the calculated F98N-apoflavodoxin structure superposed over the same regions in the crystalline structure of the wild-type protein. Backbone atoms for wild-type apoflavodoxin are displayed in black. (d) Hydrophobic cluster between helices α1 and α5 (in green) and strands β1 and β3 (in cyan) in the NMR structure of F98N apoflavodoxin superimposed on the corresponding cluster in the crystalline wild-type apoflavodoxin (in black). Side chains in the cluster are colored following the same color code.

solution,[27,28] and it has been especially useful for the structural characterization of unfolded and partially unfolded states of proteins.[29,30] We have performed a SAXS study of F98N to address the overall structural features of this mutant and to quantify the differences with respect to the wild type (see Materials and Methods). Guinier's analysis of the initial part of F98N SAXS curve (Fig. 5a) yielded a radius of gyration (R_g) of 18.3±0.2 Å for this apoflavodoxin mutant. The forward scattering, $I(0)$, also obtained using Guinier's approach, indicates that the SAXS profile originates from a particle of 18±2 kDa (theoretical molecular mass is 18.8 kDa), demonstrating the monomeric nature of the protein in solution. The distance distribution function, $p(r)$, calculated from the scattering profile using a Fourier transform, presents a pronounced peak, which indicates that the mutant adopts a globular shape with a maximum distance within the particle, D_{max}, of 61±3 Å (Fig. 5b). In contrast, the R_g and D_{max} calculated from the wild-type structure are notably smaller, 15.75 Å and 45±2 Å (Fig. 5b),

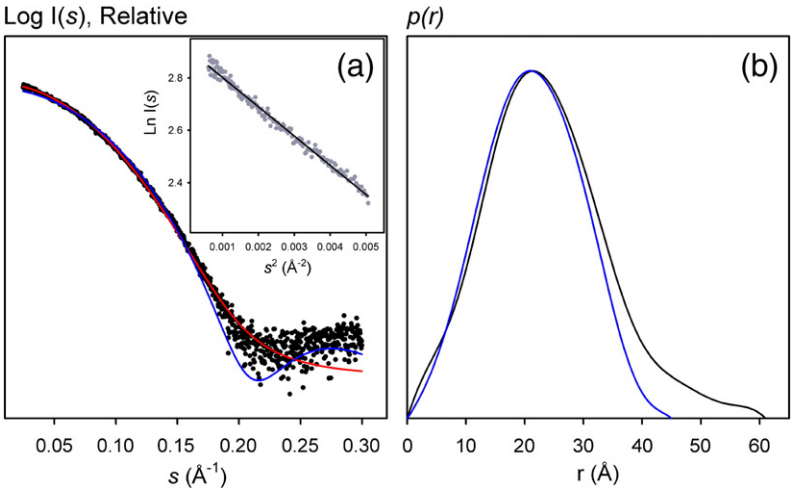

Fig. 5. SAXS analysis of the F98N apoflavodoxin point mutant. (a) Scattering intensity in logarithmic scale (black dots) as a function of the momentum transfer $s = 4\pi\sin(\theta)/\lambda$, where $\lambda = 1.5$ Å is the X-ray wavelength and 2θ is the scattering angle. Fitted curve with the NMR structure with lowest energy (red) and the apoflavodoxin crystallographic structure (blue) are displayed as continuous lines. A momentum transfer range of $0.025 < s < 0.3$ Å^{-1} was used for CRYSOL fits. Guinier's fit to the initial part of the curve is displayed in the inset. (b) Distance distribution function, $p(r)$, calculated with GNOM using the SAXS profile measured for F98N (black) compared to that computed from the apoflavodoxin crystallographic structure (blue). Normalized values of $p(r)$ are displayed with their maximum values being 1.

respectively. Therefore, according to SAXS data, the F98N mutant adopts a globular structure, characteristic of folded polypeptides, but presents conformations that are more extended than native wild-type apoflavodoxin.

The accuracy of the F98N structural model derived from NMR has been validated using the SAXS curve measured in the same experimental conditions. The 20 NMR structures were fitted to the SAXS profile using CRYSOL[31] and good fits were obtained for all of them. To exemplify this observation, the fit to the lowest-energy NMR structure with a $\chi = 1.04$ is displayed in Fig. 5a. When fitting the experimental curve to the crystallographic structure of apoflavodoxin (1FTG), a notably worse fit was obtained, $\chi = 1.44$, with noticeable departures in the initial part and in the higher-resolution section, around $s = 0.2$ Å^{-1}, of the curve. These results suggest that the F98N mutant adopts a slightly larger and less compact structure in solution than the crystallographic model of the wild type. SAXS analysis thus validates the high-resolution structural models derived by NMR and substantiates their enhanced degree of expansion relative to the native structure.

Discussion

Obtaining a good model of the partly unfolded equilibrium intermediate of apoflavodoxin

Characterizing the structure of a partly unfolded protein is a laborious task that is further complicated when the partly unfolded conformation appears mixed with significant amounts of fully folded and/or fully unfolded protein populations. The equilibrium intermediate observed in the thermal unfolding of apoflavodoxin[13] is one of the several partly unfolded conformations described for this protein. The qualitative structural model of the intermediate arising from equilibrium φ-analysis[4] is composed of a large native-like region and an unfolded region comprising discontinuous sequence segments adjacent in the native structure of the protein.[32] Thus, the thermal intermediate does not resemble either the molten globule conformation of the protein that accumulates at low pH,[33] which has been best characterized in truncated forms of the protein,[21,34] or the transition state of the folding reaction.[22] On the other hand, it is not known whether it is similar to the transient intermediate observed in the folding reaction.[23] However, its free energy is only slightly higher than that of the native state,[14] which allows the intermediate to become the most stable species when the temperature is raised and even at lower temperatures in some point mutants. On the other hand, the disordered regions of the intermediate appear to overlap with the recognition sites for the FMN cofactor and for partner proteins.[16,35,36] Due to its energetic proximity to the native state, the intermediate could transiently populate at ambient temperatures and play a functional role in ligand binding.

Obtaining high-resolution structural data of equilibrium intermediates belonging to the native ensemble, such as this one, is important for understanding native-state protein dynamics. A point mutant that destabilizes the native conformation of wild-type apoflavodoxin relative to the intermediate so that the intermediate becomes the only conformation significantly populated at 25 °C was designed on the basis of previously reported equilibrium φ-analysis data.[14] According to it, a cluster formed by four aromatic residues is located right in the native inner interface that is destabilized in the intermediate and becomes exposed to solvent. We have replaced F98, one of the residues involved in the aromatic cluster, by the shorter, polar asparagine. The mutant is expressed and purified with good yields and displays spectroscopic

properties that are in good agreement with those exhibited by the wild-type thermal intermediate. Significantly, unlike wild-type apoflavodoxin and tens of mutants thereof previously analyzed in the laboratory that showed three-state thermal unfolding,[14] the F98N mutant is two-state, and the thermodynamic parameters of the unfolding are similar to those of the I-to-U unfolding transition of wild type (Table 1). All the evidence gathered indicates that the F98N mutant adopts at 25 °C a structure similar to that of the equilibrium intermediate of the thermal unfolding of wild-type apoflavodoxin. Importantly, the two-state thermal unfolding equilibrium together with the relatively high temperature of mid-denaturation of the F98N mutant determines that the populations of fully folded and fully unfolded molecules are negligible at 25 °C, and therefore, the mutant populates at this temperature a single conformation (more precisely, a single ensemble), which facilitates NMR and SAXS analysis.

The solution structure of the model intermediate delineates the native and disordered regions at atomic resolution

The NMR data indicate that the structure ensemble populated by F98N at 25 °C contains two very different regions. One is a well-defined compact domain formed by five noncontiguous segments of the protein chain that fold together. This folded domain maintains all the regular secondary-structure elements of native apoflavodoxin, except for strand β5b, which is not formed (Fig. 4c). The secondary-structure 3D arrangement is native-like and consists of a five-stranded parallel β-sheet surrounded by helices α1 and α5, packed together onto one side of the sheet, and by helices α2, α3, and α4, packed onto the opposite side (Fig. 4). In this folded domain, strand β4 and helices α4 and α5 are shorter than those in the native protein. The structure of this compact domain is very similar to that of the corresponding segments of the native wild-type protein. In particular, it is of note that the hydrophobic clusters formed in the wild-type protein between the parallel β-sheet and the two groups of helices are essentially preserved (Fig. 4d). The disordered region of F98N encompasses two loops spatially close in the structure of native apoflavodoxin: the loop connecting strand β4 and helix α4 (11 residues long) and the 23-residue loop that splits strand β5 into two segments, β5a and β5b, which is characteristic of long-chain flavodoxins. In the wild-type thermal intermediate, both loops were also described as unfolded from equilibrium φ-value analysis.[14]

On the whole, the high-resolution structure determined here for the apoflavodoxin thermal intermediate agrees well with the qualitative structural model deduced from equilibrium φ-analysis.[14] However, while the previous model represented a very coarse-grained qualitative division of the protein into native and unfolded regions, the solution structure now reported provides atomic-level detail for the folded domain, and importantly, it delineates precisely the boundary between the native and the unfolded regions.

Conformational expansion evidenced by SAXS and NMR solution structures for the intermediate are in agreement

SAXS is a highly complementary technique to NMR as it is sensitive to the overall properties of molecules in solution in contrast to the local nature of most NMR structural parameters.[37–39] This synergy is especially relevant for flexible systems where the degree of conformational expansion can be monitored by SAXS curves.[40,41] SAXS confirms that F98N presents a mainly globular structure that, according to the R_g and D_{max} values derived from the curve, displays a moderate conformational expansion, which is incompatible with the crystallographic structure of the wild-type protein. However, the degree of conformational expansion is consistent with the calculated NMR ensemble (Fig. 4b). Thus, SAXS profile validates the F98N apoflavodoxin NMR structure.

Singularity of the protein inner interface involved in the native-to-intermediate transition: A link between thermally activated native regions and natively unfolded proteins?

There is mounting evidence that non-native conformations close to the native basin may be important for function.[1–3] Since these conformations may be transiently populated without the folded protein having to make long excursions from the stability minimum of the native state, they could get involved in ligand recognition or catalysis. The thermal intermediate of flavodoxins[14,16] is one such conformation, and links between the function and dynamics of flavoproteins abound.[42] The involvement of the two flavodoxin segments that become unfolded in the intermediate in ligand recognition is clear. The first segment (87–108) includes one of the loops that bind the FMN redox cofactor,[32] and it has been demonstrated that the primary recognition event between apoflavodoxin and FMN involves a tyrosine residue of the loop.[43] On the other hand, a variety of flavodoxin partners, including flavodoxin reductase, cobalamin-dependent methionine synthase, and protoporphyrinogen, appear to bind at the second segment (118–152).[35,36]

Structural analysis of equilibrium intermediates is a powerful tool to identify the regions of a given protein that will engage in functionally relevant dynamical processes. Based on the qualitative structural model of the apoflavodoxin intermediate derived from equilibrium φ-value analysis,[14] we suggested that such regions could be related with structural elements that pack to form non-very apolar inner interfaces. We are now quantitatively testing this hypothesis in flavodoxin and other proteins by deriving polarity profiles for internal

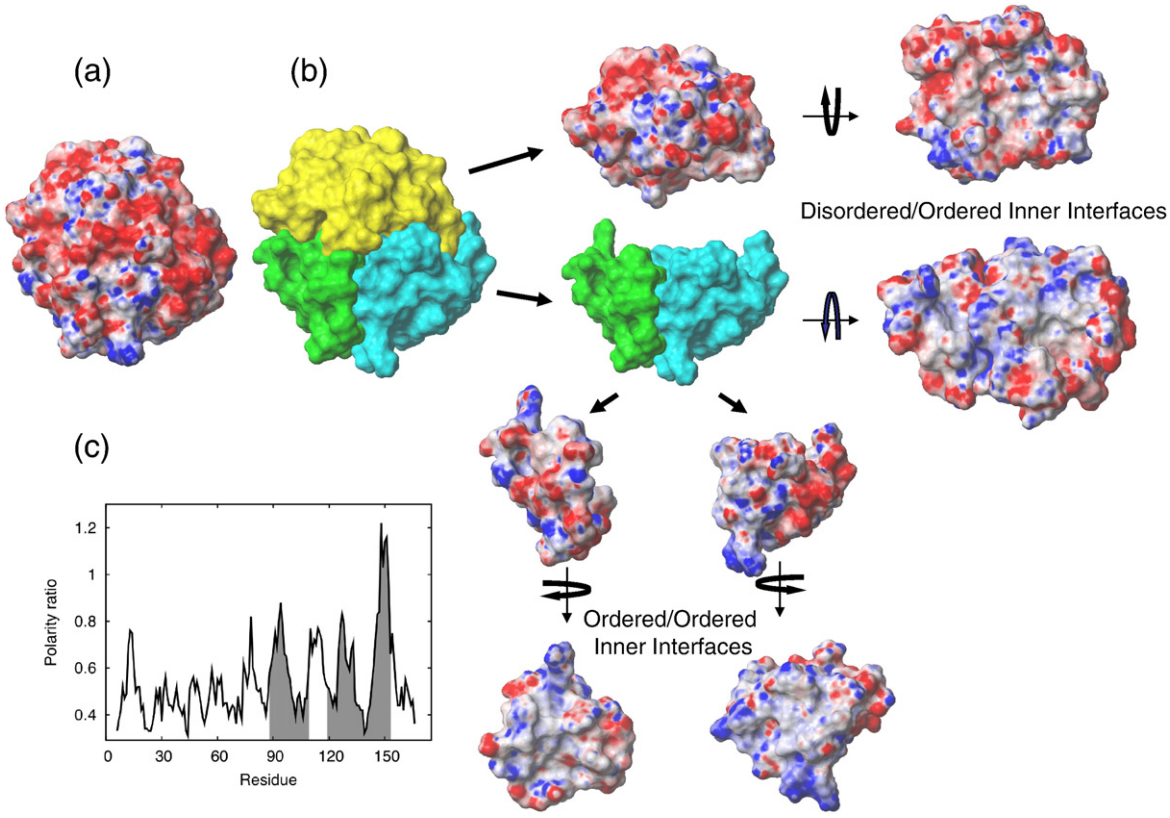

Fig. 6. Polarity of wild-type apoflavodoxin inner interfaces. (a) Electrostatic surface of wild-type apoflavodoxin (PDB code: 1FTG), orientation as in Fig. 4a. (b) Apoflavodoxin structure was divided first into two halves corresponding, respectively, to the disordered (in yellow) and well-folded (in green–cyan) regions in the thermal intermediate (Fig. 4b). These two halves are rotated about 90°, as indicated, to display front views of the inner electrostatic surfaces between disordered and ordered regions. The half comprising the well-folded region in the thermal intermediate was further subdivided into two sections: one comprising helices α1 and α5 (in green) and the other one comprising the β-sheet and the ordered segments of helices α2, α3, and α4 (in cyan; Fig. 4a). These two sections are rotated approximately 90°, as indicated, to exhibit front views of the inner electrostatic surfaces illustrating the low polarity characteristic of the inner interfaces in protein cores. (c) The ratio of polar over apolar surface buried in the intra-faces formed by segments of eight consecutive residues and the rest of the protein has been calculated for the 3D apoflavodoxin structure (PDB code: 1FTG). Surface-accessible areas were determined using NACCESS.[44] Details on the calculation will be published elsewhere. The 87–107 and 118–143 segments encompassing the regions that become unfolded in the transition from native to intermediate are shadowed in gray to highlight their correspondence with regions having inner interfaces exhibiting a high polar/apolar ratio.

protein interfaces (V.E.A. and J.S., unpublished results). The apoflavodoxin polarity profile is shown in Fig. 6c where the protein internal interfaces are characterized by the ratio between the polar and apolar areas that are buried in order to form them (excluding the area buried within the window sequence). As the figure clearly shows, the two dynamic segments of the apoflavodoxin thermal intermediate correspond to regions exhibiting high polar/apolar ratios and thus establishing more polar interfaces with the rest of the protein than other regions. This observation quantitatively indicates that the interface in the boundary between the folded and the unfolded regions in the thermal intermediate is unusually polar. This fact can be qualitatively visualized by splitting the native apoflavodoxin structure into two halves and looking at the inner electrostatic surfaces (Fig. 6a and b). Indeed, the electrostatic surface of the well-folded region in the thermal intermediate (Figs. 4b and 6a and b) displays a fairly even distribution, where the surface in contact with the disordered region is only slightly less polar than the outer surfaces. Similarly, the inner interface shown by the disordered region when it appears folded in the native structure is rather polar (Fig. 6a and b). In contrast, two halves resulting from cutting the ordered region of the thermal intermediate exhibit quite apolar inner electrostatic surfaces (Fig. 6a and b). Apolar inner interfaces are characteristic of natively folded proteins, typically organized around cores formed by the packing of hydrophobic surfaces provided by interacting protein segments. At the other extreme, natively unfolded proteins are rich in polar residues[5] unsuitable to form hydrophobic cores, and they do not attain compact folds unless they bind to ligand partners that compensate this stability deficit. Hence, we speculate that, as in the apoflavodoxin case (Fig. 6), the dynamic regions of natively folded proteins are very likely characterized

by forming cores of an intermediate level of hydrophobicity that are mildly stable at physiological temperatures but easily responsive to thermal activation.

Materials and Methods

Mutagenesis, protein expression, labeling, and purification

PCR mutagenesis of the *Anabaena* PCC 7119 gene was performed as described in the Stratagene QuikChange Kit. The F98N mutation was identified by sequencing. The flavodoxin gene[45] was expressed in *Escherichia coli*. ^{15}N-enriched protein was obtained using $^{15}NH_4Cl$ as the sole nitrogen source in the growth medium. Flavodoxin was purified and its FMN cofactor removed to get the apo form as previously described.[33]

Circular dichroism

CD spectra of wild-type and mutant apoflavodoxin were carried out in Jasco 710 or Chirascan (from Applied Photophysics) spectropolarimeters. Near-UV spectra in 50 mM Mops, pH 7, were recorded from 260 to 310 nm in a 4-mm-path-length cuvette using 30 μM protein solutions. Far-UV spectra in 5 mM Mops, pH 7 (plus 15 mM NaCl), were measured from 200 to 250 nm in a 1-mm-path-length cuvette, using 15 μM protein solutions.

Spectra deconvolution

The spectroscopic properties of the macroscopic states of *Anabaena* apoflavodoxin that become populated during the thermal unfolding have been determined by deconvolution of spectra recorded at different temperatures, using the following equation:

$$Y(\lambda,T) = Y_N(\lambda,T)X_N(T) + Y_I(\lambda,T)X_I(T) + Y_U(\lambda,T)X_U(T) \quad (1)$$

where the observed value of a spectroscopic signal at a given wavelength and temperature, Y(λ,T), is a linear combination of the values of the different states, $Y_i(\lambda,T)$ and of their populations, $X_i(T)$. The latter are calculated at each temperature from the free-energy values ΔG_1 and ΔG_2 obtained by global fitting of the unfolding curves to the sequential three-state model.

Thermal unfolding curves

Wild-type and mutant apoflavodoxin thermal unfolding curves in 50 mM mops, pH 7, were followed from approximately 278 to 363 K by far-UV CD (222 nm; 30 μM protein, 1 mm path length), near-UV CD and near-UV absorbance (291 nm; 30 μM protein, 4 mm path-length), and near-UV fluorescence emission (excitation at 280 nm; emission ratio of 320 over 360 nm; 2 μM protein). To identify the number of thermodynamic states that populate in the unfolding equilibrium, we subjected the four curves recorded for each protein to global analysis. To allow all curves to contribute similarly to the fit, they are roughly normalized to similar property value spans of approximately 1 to 0. The four curves of a given variant are then globally fitted to common ΔH, T_m and ΔC_p values, using the Origin 7.0 program (OriginLab Corporation) and either three-state or two-state equations. In contrast to the wild-type apoflavodoxin thermal unfolding, which is three-state,[13,14] that of the F98N mutant is best described by a two-state model. Accordingly, the F98N unfolding curves were analyzed using the following equation:[46,47]

$$Y = \frac{(Y_N + m_N Y) + (Y_D + m_D T)e^{-\left(\Delta H(1-T/T_m) - \Delta C_p((T_m - T) + T\ln(T/T_m))\right)/RT}}{1 + e^{-\left(\Delta H(1-T/T_m) - \Delta C_p((T_m - T) + T\ln(T/T_m))\right)/RT}} \quad (2)$$

where Y is the spectroscopic signal, Y_N and Y_D are the signals of the native and denatured states (m_N and m_D being the slopes that describe their dependences with temperature), T_m is the transition temperature, and ΔH and ΔC_p are the enthalpy and specific heat of denaturation at T_m, respectively.

Differential scanning calorimetry

The heat capacities of wild-type and F98N apoflavodoxins were measured as a function of temperature with a high-precision differential scanning VP-DSC microcalorimeter (Microcal LLC, Northampton, MA). Protein samples and reference solutions were properly degassed and carefully loaded into the cells to avoid bubble formation. The baseline of the instrument was routinely recorded before the experiments with both cells filled with buffer. Thermal denaturation scans of apoflavodoxin were performed with 50 μM protein solutions in 50 mM Mops, pH 7.0, at a scanning rate of 1 °C/min from 10 to 100 °C. Reversibility of the unfolding was checked by sample reheating after cooling inside the calorimetric cell. DSC data analysis was performed by using a two-state or a three-state model in Origin 7.0 software package (OriginLab Corporation).

NMR spectroscopy

Protein samples for NMR experiments were approximately 1 mM in 0.5 ml of 5 mM phosphate buffer at pH 7.0 in either H_2O/D_2O (9:1 ratio by volume) or pure D_2O. pH was measured with a glass micro electrode and was not corrected for isotope effects. Both the pH and the ionic strength of this buffer are very similar to those of the buffer used for the stability and spectroscopic characterization of F98N. Therefore, the stability of the protein in either buffer is very similar and the same species are populated in either buffer at a given temperature. The temperature of the NMR probe was calibrated using a methanol sample. NMR experiments were recorded at 25 °C on a Bruker AV 600-MHz spectrometer equipped with a *z*-gradient cryoprobe. Sodium 2,2-dimethyl-2-silapentane-5-sulfonate was used as an internal chemical shift reference. The 0-ppm ^{13}C and ^{15}N δ values were obtained indirectly by multiplying the spectrometer frequency that corresponds to 0 ppm in the ^{1}H spectrum, assigned to internal 2,2-dimethyl-2-silapentane-5-sulfonate reference, by 0.251449530 and 0.101329118, respectively.[48] Two- and three-dimensional NMR spectra were acquired by using standard pulse sequences. All the NMR spectra were processed using XWIN-NMR/TOPSPIN software (Bruker Biospin, Karlsruhe, Germany) and analyzed with Sparky (T. D. Goddard and D. G. Kneller, Sparky 3, University of California, San Francisco, USA).

NMR assignment

^{1}H and ^{15}N resonances of *Anabaena* F98N-apoflavodoxin were assigned by the standard sequence-specific method.[49] 3D HNHA and 120-ms ^{15}N-NOESY-HSQC spectrum recorded on a ^{15}N-labeled sample in H_2O/D_2O 9:1 v/v were analyzed together with 2D correlated spectroscopy, 60 ms total correlated spectroscopy, and 120 ms NOESY spectra of the unlabeled protein in both H_2O/D_2O 9:1 v/v and D_2O. Some ^{13}C chemical shifts were assigned on the basis of a ^{1}H–^{13}C-HSQC recorded at natural ^{13}C abundance for the unlabeled protein in D_2O. The assignment of the F98N mutant was facilitated by the available ^{1}H, ^{15}N, and ^{13}C chemical shifts for native apoflavodoxin [Biological Magnetic Resonance Data Bank (BioMagResBank) code: BMRB-5011].[26] The chemical shifts assigned for F98N apoflavodoxin have been deposited in the BioMagResBank (accession code: BMRB-16593†).

Structure calculation

NOE-derived distance constraints were derived from two 2D NOESY spectra, one recorded in H_2O/D_2O 9:1 v/v and the other in D_2O. ϕ and ψ angle restraints were obtained from $^{1}H^{\alpha}$ chemical shifts by using the TALOS program.[50] Structures were calculated using the program CYANA and the CANDID protocol for iterative automatic NOE assignment.[51] The standard protocol was used with seven cycles of combined automated NOE assignment and structure calculation of 100 conformers in each cycle, from which the 20 structures with lowest target function value were selected for further analysis. A final restricted molecular dynamics step was applied to the 20 structures resulting from the seventh cycle. These structures have been deposited at the Protein Data Bank (PDB) under code 2KQU.

Structure analysis

Structures were analyzed with the program MOLMOL[52] and PROCHECK/NMR.[53] A side-chain torsion angle was considered as well defined when the RMSD between values in the best 20 calculated structures is less than ±30° or its order parameter is in the range 0.87–1.00 (the order parameter is 0 for a totally random dihedral angle and 1 for a completely fixed conformation). Electrostatic surfaces were calculated using MOLMOL.[52]

SAXS measurements

SAXS data were collected at X33 beamline at the European Molecular Biology Laboratory in the storage ring DORIS III of the Deutsches Elektronen-Synchrotron (Hamburg).[54] Scattering curves of F98N apoflavodoxin mutant were measured at 25 °C at protein concentrations of 6.7, 4.0, and 2.0 mg/ml at pH 7 and an exposure time of 2 min. The scattering profiles covered a range of momentum transfer of $0.007 < s < 0.63$ Å^{-1}. Radiation damage was monitored by repetitive 30-s exposures, and no significant changes were observed. Buffer scattering profiles were measured before and after the samples; they were averaged and used for the subtraction from the protein scattering profiles. The curves measured at the three concentrations were merged and converted to a single curve that was used for structural analysis. All data manipulations were done using standard procedures with the software PRIMUS.[55]

The forward scattering, $I(0)$, and the radius of gyration, R_g, were evaluated using the Guinier's approximation,[56] assuming that at very small angles ($s < 1.3/R_g$), the intensity can be well represented as $I(s) = I(0)\exp(-(sR_g)^2/3)$. The apparent molecular weights of the proteins were estimated from their forward scattering, $I(0)$, by comparison to the one obtained for a bovine serum albumin sample of 4.5 mg/ml. The maximum particle dimensions, D_{max}, and the distance distribution function, $p(r)$, were computed with the program GNOM[57] using a momentum transfer range of $0.025 < s < 0.50$ Å^{-1}. The agreement between the profile with the NMR and the crystallographic (1FTG) structures was evaluated with CRYSOL.[31]

Accession numbers

Coordinates have been deposited in the PDB with accession number 2KQU. Chemical shifts have been deposited at the BioMagResBank with accession code 16593.

Acknowledgements

We thank Prof. M. Rico for helpful and encouraging comments on the manuscript. N. Jiménez-Menéndez and A. Rubio (Instituto de Biología Molecular de Barcelona) are thanked for some of the SAXS measurements. We acknowledge financial support from grants BFU2007-61376 [Ministerio de Ciencia e Innovacion (MICINN), Spain] and PI078/08 (DGA, Spain) to J.S., from grant CTQ2008-00080/BQU (MICINN, Spain) to M.A.J., and from EU (RII/2004/5060008 to the European Molecular Biology Laboratory, Hamburg). S.A.-T. was supported by an FPI fellowship (MICINN-FSE, Spain) and V.E.A. was funded by Banco Santander Central Hispano, Fundación Carolina, and Universidad de Zaragoza, and is now recipient of a CSIC fellowship (JAEpre program). P.B. holds a Ramón y Cajal contract partially financed by the Spanish MEC.

Supplementary Data

Supplementary data associated with this article can be found, in the online version, at doi:10.1016/j.jmb.2010.05.050

References

1. Erickson, J. A., Jalaie, M., Robertson, D. H., Lewis, R. A. & Vieth, M. (2004). Lessons in molecular recognition: the effects of ligand and protein flexibility on molecular docking accuracy. *J. Med. Chem.* **47**, 45–55.
2. Bahar, I., Chennubhotla, C. & Tobi, D. (2007). Intrinsic dynamics of enzymes in the unbound state and relation to allosteric regulation. *Curr. Opin. Struct. Biol.* **17**, 633–640.

† http://www.bmrb.wisc.edu

3. De Simone, A., Richter, B., Salvatella, X. & Vendruscolo, M. (2009). Toward an accurate determination of free energy landscapes in solution states of proteins. *J. Am. Chem. Soc.* **131**, 3810–3811.
4. Cremades, N., Sancho, J. & Freire, E. (2006). The native-state ensemble of proteins provides clues for folding, misfolding and function. *Trends Biochem. Sci.* **31**, 494–496.
5. Dyson, H. J. & Wright, P. E. (2004). Unfolded proteins and protein folding studied by NMR. *Chem. Rev.* **104**, 3607–3622.
6. Korzhnev, D. M., Salvatella, X., Vendruscolo, M., Di Nardo, A. A., Davidson, A. R., Dobson, C. M. & Kay, L. E. (2004). Low-populated folding intermediates of Fyn SH3 characterized by relaxation dispersion NMR. *Nature*, **430**, 586–590.
7. Redfield, C. (2004). Using nuclear magnetic resonance spectroscopy to study molten globule states of proteins. *Methods*, **34**, 121–132.
8. Vallurupalli, P., Hansen, D. F., Stollar, E., Meirovitch, E. & Kay, L. E. (2007). Measurement of bond vector orientations in invisible excited states of proteins. *Proc. Natl Acad. Sci. USA*, **104**, 18473–18477.
9. Whittaker, S. B., Spence, G. R., Gunter Grossmann, J., Radford, S. E. & Moore, G. R. (2007). NMR analysis of the conformational properties of the trapped on-pathway folding intermediate of the bacterial immunity protein Im7. *J. Mol. Biol.* **366**, 1001–1015.
10. Religa, T. L., Markson, J. S., Mayor, U., Freund, S. M. & Fersht, A. R. (2005). Solution structure of a protein denatured state and folding intermediate. *Nature*, **437**, 1053–1056.
11. Uzawa, T., Nishimura, C., Akiyama, S., Ishimori, K., Takahashi, S., Dyson, H. J. & Wright, P. E. (2008). Hierarchical folding mechanism of apomyoglobin revealed by ultra-fast H/D exchange coupled with 2D NMR. *Proc. Natl Acad. Sci. USA*, **105**, 13859–13864.
12. Nishimura, C., Dyson, H. J. & Wright, P. E. (2010). Energetic frustration of apomyoglobin folding: role of the B helix. *J. Mol. Biol.* **396**, 1319–1328.
13. Irun, M. P., Garcia-Mira, M. M., Sanchez-Ruiz, J. M. & Sancho, J. (2001). Native hydrogen bonds in a molten globule: the apoflavodoxin thermal intermediate. *J. Mol. Biol.* **306**, 877–888.
14. Campos, L. A., Bueno, M., Lopez-Llano, J., Jimenez, M. A. & Sancho, J. (2004). Structure of stable protein folding intermediates by equilibrium phi-analysis: the apoflavodoxin thermal intermediate. *J. Mol. Biol.* **344**, 239–255.
15. Yan, S., Gawlak, G., Smith, J., Silver, L., Koide, A. & Koide, S. (2004). Conformational heterogeneity of an equilibrium folding intermediate quantified and mapped by scanning mutagenesis. *J. Mol. Biol.* **338**, 811–825.
16. Sancho, J. (2006). Flavodoxins: sequence, folding, binding, function and beyond. *Cell. Mol. Life Sci.* **63**, 855–864.
17. Irun, M. P., Maldonado, S. & Sancho, J. (2001). Stabilization of apoflavodoxin by replacing hydrogen-bonded charged Asp or Glu residues by the neutral isosteric Asn or Gln. *Protein Eng.* **14**, 173–181.
18. Cremades, N., Velazquez-Campoy, A., Freire, E. & Sancho, J. (2008). The flavodoxin from *Helicobacter pylori*: structural determinants of thermostability and FMN cofactor binding. *Biochemistry*, **47**, 627–639.
19. Cremades, N. & Sancho, J. (2008). Molten globule and native state ensemble of *Helicobacter pylori* flavodoxin: can crowding, osmolytes or cofactors stabilize the native conformation relative to the molten globule? *Biophys. J.* **95**, 1913–1927.
20. Bollen, Y. J., Kamphuis, M. B. & van Mierlo, C. P. (2006). The folding energy landscape of apoflavodoxin is rugged: hydrogen exchange reveals nonproductive misfolded intermediates. *Proc. Natl Acad. Sci. USA*, **103**, 4095–4100.
21. Lopez-Llano, J., Campos, L. A., Bueno, M. & Sancho, J. (2006). Equilibrium phi-analysis of a molten globule: the 1–149 apoflavodoxin fragment. *J. Mol. Biol.* **356**, 354–366.
22. Bueno, M., Ayuso-Tejedor, S. & Sancho, J. (2006). Do proteins with similar folds have similar transition state structures? A diffuse transition state of the 169 residue apoflavodoxin. *J. Mol. Biol.* **359**, 813–824.
23. Fernandez-Recio, J., Genzor, C. G. & Sancho, J. (2001). Apoflavodoxin folding mechanism: an alpha/beta protein with an essentially off-pathway intermediate. *Biochemistry*, **40**, 15234–15245.
24. Lopez-Llano, J., Maldonado, S., Bueno, M., Lostao, A., Angeles-Jimenez, M., Lillo, M. P. & Sancho, J. (2004). The long and short flavodoxins: I. The role of the differentiating loop in apoflavodoxin structure and FMN binding. *J. Biol. Chem.* **279**, 47177–47183.
25. Lopez-Llano, J., Maldonado, S., Jain, S., Lostao, A., Godoy-Ruiz, R., Sanchez-Ruiz, J. M. *et al.* (2004). The long and short flavodoxins: II. The role of the differentiating loop in apoflavodoxin stability and folding mechanism. *J. Biol. Chem.* **279**, 47184–47191.
26. Langdon, G. M., Jimenez, M. A., Genzor, C. G., Maldonado, S., Sancho, J. & Rico, M. (2001). *Anabaena* apoflavodoxin hydrogen exchange: on the stable exchange core of the alpha/beta(21345) flavodoxin-like family. *Proteins*, **43**, 476–488.
27. Petoukhov, M. V. & Svergun, D. I. (2007). Analysis of X-ray and neutron scattering from biomacromolecular solutions. *Curr. Opin. Struct. Biol.* **17**, 562–571.
28. Koch, M. H., Vachette, P. & Svergun, D. I. (2003). Small-angle scattering: a view on the properties, structures and structural changes of biological macromolecules in solution. *Q. Rev. Biophys.* **36**, 147–227.
29. Bernado, P., Mylonas, E., Petoukhov, M. V., Blackledge, M. & Svergun, D. I. (2007). Structural characterization of flexible proteins using small-angle X-ray scattering. *J. Am. Chem. Soc.* **129**, 5656–5664.
30. Doniach, S. (2001). Changes in biomolecular conformation seen by small angle X-ray scattering. *Chem. Rev.* **101**, 1763–1778.
31. Svergun, D., Barberato, C. & Koch, M. H. J. (1995). CRYSOL—a program to evaluate x-ray solution scattering of biological macromolecules from atomic coordinates. *J. Appl. Crystallogr.* **28**, 768–773.
32. Genzor, C. G., Perales-Alcon, A., Sancho, J. & Romero, A. (1996). Closure of a tyrosine/tryptophan aromatic gate leads to a compact fold in apo flavodoxin. *Nat. Struct. Biol.* **3**, 329–332.
33. Genzor, C. G., Beldarrain, A., Gomez-Moreno, C., Lopez-Lacomba, J. L., Cortijo, M. & Sancho, J. (1996). Conformational stability of apoflavodoxin. *Protein Sci.* **5**, 1376–1388.
34. Maldonado, S., Jimenez, M. A., Langdon, G. M. & Sancho, J. (1998). Cooperative stabilization of a molten globule apoflavodoxin fragment. *Biochemistry*, **37**, 10589–10596.
35. Boynton, T. O., Daugherty, L. E., Dailey, T. A. & Dailey, H. A. (2009). Identification of *Escherichia coli* HemG as a novel, menadione-dependent flavodoxin with protoporphyrinogen oxidase activity. *Biochemistry*, **48**, 6705–6711.

36. Hall, D. A., Vander Kooi, C. W., Stasik, C. N., Stevens, S. Y., Zuiderweg, E. R. & Matthews, R. G. (2001). Mapping the interactions between flavodoxin and its physiological partners flavodoxin reductase and cobalamin-dependent methionine synthase. *Proc. Natl Acad. Sci. USA*, **98**, 9521–9526.
37. Sunnerhagen, M., Olah, G. A., Stenflo, J., Forsen, S., Drakenberg, T. & Trewhella, J. (1996). The relative orientation of Gla and EGF domains in coagulation factor X is altered by Ca^{2+} binding to the first EGF domain. A combined NMR-small angle X-ray scattering study. *Biochemistry*, **35**, 11547–11559.
38. Mattinen, M. L., Paakkonen, K., Ikonen, T., Craven, J., Drakenberg, T., Serimaa, R. *et al.* (2002). Quaternary structure built from subunits combining NMR and small-angle x-ray scattering data. *Biophys. J.* **83**, 1177–1183.
39. Grishaev, A., Wu, J., Trewhella, J. & Bax, A. (2005). Refinement of multidomain protein structures by combination of solution small-angle X-ray scattering and NMR data. *J. Am. Chem. Soc.* **127**, 16621–16628.
40. Bernado, P., Blanchard, L., Timmins, P., Marion, D., Ruigrok, R. W. & Blackledge, M. (2005). A structural model for unfolded proteins from residual dipolar couplings and small-angle x-ray scattering. *Proc. Natl Acad. Sci. USA*, **102**, 17002–17007.
41. Wells, M., Tidow, H., Rutherford, T. J., Markwick, P., Jensen, M. R., Mylonas, E. *et al.* (2008). Structure of tumor suppressor p53 and its intrinsically disordered N-terminal transactivation domain. *Proc. Natl Acad. Sci. USA*, **105**, 5762–5767.
42. Senda, T., Senda, M., Kimura, S. & Ishida, T. (2009). Redox control of protein conformation in flavoproteins. *Antioxid. Redox Signal.* **11**, 1741–1766.
43. Lostao, A., Daoudi, F., Irun, M. P., Ramon, A., Fernandez-Cabrera, C., Romero, A. & Sancho, J. (2003). How FMN binds to *Anabaena* apoflavodoxin: a hydrophobic encounter at an open binding site. *J. Biol. Chem.* **278**, 24053–24061.
44. Hubbard, S. J. & Thornton, J. M. (1993). *NACCESS Computer Program Department of Biochemistry and Molecular Biology.* University College London, London, UK.
45. Fillat, M. F., Borrias, W. E. & Weisbeek, P. J. (1991). Isolation and overexpression in *Escherichia coli* of the flavodoxin gene from *Anabaena* PCC 7119. *Biochem. J.* **280**, 187–191.
46. Privalov, P. L. (1979). Stability of proteins: small globular proteins. *Adv. Protein Chem.* **33**, 167–241.
47. Privalov, P. L. & Potekhin, S. A. (1986). Scanning microcalorimetry in studying temperature-induced changes in proteins. *Methods Enzymol.* **131**, 4–51.
48. Markley, J. L., Bax, A., Arata, Y., Hilbers, C. W., Kaptein, R., Sykes, B. D. *et al.* (1998). IUPAC–IUBMB–IUPAB inter-union task group on the standardization of data bases of protein and nucleic acid structures determined by NMR spectroscopy. *Pure Appl. Chem.* **70**, 117–142.
49. Wuthrich, K., Billeter, M. & Braun, W. (1984). Polypeptide secondary structure determination by nuclear magnetic resonance observation of short proton–proton distances. *J. Mol. Biol.* **180**, 715–740.
50. Cornilescu, G., Delaglio, F. & Bax, A. (1999). Protein backbone angle restraints from searching a database for chemical shift and sequence homology. *J. Biomol. NMR*, **13**, 289–302.
51. Guntert, P., Mumenthaler, C. & Wuthrich, K. (1997). Torsion angle dynamics for NMR structure calculation with the new program DYANA. *J. Mol. Biol.* **273**, 283–298.
52. Koradi, R., Billeter, M. & Wuthrich, K. (1996). MOLMOL: a program for display and analysis of macromolecular structures. *J. Mol. Graphics* 14, 51–55, 29–32.
53. Laskowski, R. A., Rullmannn, J. A., MacArthur, M. W., Kaptein, R. & Thornton, J. M. (1996). AQUA and PROCHECK-NMR: programs for checking the quality of protein structures solved by NMR. *J. Biomol. NMR*, **8**, 477–486.
54. Roessle, M. W., Klaering, R., Ristau, U., Robrahn, B., Jahn, D., Gehrmann, T. *et al.* (2007). Upgrade of the small angle X-ray scattering beamline X33 at the European Molecular Biology Laboratory, Hamburg. *J. Appl. Crystallogr.* **40**, s190–s194.
55. Konarev, P. V., Volkov, V. V., Sokolova, A. V., Koch, M. H. J. & Svergun, D. I. (2003). PRIMUS: a Windows PC-based system for small-angle scattering data analysis. *J. Appl. Crystallogr.* **36**, 1277–1282.
56. Guinier, A. (1939). La diffraction des rayons X aux très faibles angles: applications à l'etude des phénomènes ultra-microscopiques. *Ann. Phys. (Paris)*, **12**, 161–237.
57. Svergun, D. I. (1992). Determination of the regularization parameter in indirect-transform methods using perceptual criteria. *J. Appl. Crystallogr.* **25**, 495–503.